ACCSCIENCE PUBLISHING

Eurasian Journal of Medicine and Oncology

ORIGINAL RESEARCH ARTICLE

Influence of tumor mutational burden and immune infiltration on cervical squamous cell carcinoma prognosis

Batchimeg Tsedenbal[1†], Battogtokh Chimeddorj[2†], Shutao Tan[3], Zhenyong Yang[4], Yunfeng Dai[5], Yun Li[6], Haiqing Jia[7], Bayarmaa Enkhbat[8,9*], and Yanshuo Han[10,11*]

[1]Department of Training, Research, and Foreign Affairs, National Center for Pathology, Ulaanbaatar, Mongolia

[2]Department of Microbiology, Institute of Biomedical Sciences, Mongolian National University of Medical Sciences, Ulaanbaatar, Mongolia

[3]Department of Urology, Shengjing Hospital of China Medical University, Shenyang, Liaoning, China

[4]Department of Endocrinology, Tacheng Hospital of China Medical University, The People's Hospital of Tacheng Prefecture, Tacheng, Xinjiang, China

[5]Department of Pathology, Yingkou Fangda Hospital, Yingkou, Liaoning, China

[6]Department of Family Medicine, Tacheng Hospital of China Medical University, The People's Hospital of Tacheng Prefecture, Tacheng, Xinjiang, China

[7]Department of Gynecology, Cancer Hospital of Dalian University of Technology (Liaoning Cancer Hospital & Institute), Shenyang, Liaoning, China

[8]Department of Pathology and Forensic Medicine, School of Biomedicine, Mongolian National University of Medical Sciences, Ulaanbaatar, Mongolia

[9]Department of Pathology, Mongolia-Japan Hospital, Ulaanbaatar, Mongolia

[10]Department of Life Sciences and Pharmacy, School of Chemical Engineering, Ocean and Life Sciences, Dalian University of Technology, Panjin, Liaoning, China

[11]Department of Vascular Surgery, Central Hospital of Dalian University of Technology, Dalian, Liaoning, China

Abstract

Introduction: Cervical squamous cell carcinoma (CESC) remains a significant global health challenge for women, necessitating the discovery of precise molecular biomarkers to optimize personalized treatment and immunotherapy strategies.
Objective: Leveraging bioinformatics data from The Cancer Genome Atlas (TCGA) and the independent CGCI–HTMCP–CC cohort for external validation, this study rigorously evaluated the prognostic role of tumor mutational burden (TMB) in CESC.
Methods: Our methodology utilized standardized transcripts per million (TPM) normalization and the maximally selected rank statistics (maxstat) algorithm to establish biologically optimal TMB thresholds, moving beyond traditional median-based stratification.
Results: While somatic mutation analysis identified high frequencies in *TTN* (29%) and *PIK3CA* (27%), high TMB levels did not directly correlate with patient overall survival ($p = 0.720$). However, a marginal non-significant trend was observed between elevated TMB and advanced tumor T-staging ($p = 0.057$). Differential expression and Cox regression analyses highlighted PTGS2 as a distinctive TMB-related risk gene. Based on this, a TMB-related risk score (TMBRS) was constructed, demonstrating moderate yet consistent predictive utility (area under the curve = 0.696) across both

†*These authors contributed equally to this work.*

***Corresponding authors:**
Bayarmaa Enkhbat
(bayarmaa.e@mnums.edu.mn)
Yanshuo Han
(yanshuohan@dlut.edu.cn)

Citation: Tsedenbal B, Chimeddorj B, Tan S, *et al*. Influence of tumor mutational burden and immune infiltration on cervical squamous cell carcinoma prognosis. *Eurasian J Med Oncol.*
doi: 10.36922/EJMO026050057

Received: January 31, 2026

Revised: April 17, 2026

Accepted: May 6, 2026

Published online: August 26, 2026

primary and independent validation cohorts. Detailed immune profiling via Cell-type Identification by Estimating Relative Subsets of RNA Transcripts and Tumor Immune Estimation Resource revealed that high TMB and lower risk scores are specifically associated with increased infiltration of $CD8^+$ T cells and M1 macrophages, suggesting enhanced local immune recognition.

Conclusion: Although the clinical utility of the TMBRS is currently moderate, this research provides a critical proof of concept for the interplay among *PTGS2*, mutational load, and the tumor microenvironment, offering valuable mechanistic insights for future large-scale prospective clinical trials.

Keywords: Cervical squamous cell carcinoma; Tumor mutational burden; Bioinformatics; Immunotherapy; Cancer prognosis; *PTGS2*; Immune cell infiltration

1. Introduction

Cervical cancer ranks as the fourth most common malignancy in women globally, with squamous cell carcinoma being its predominant histological type. Approximately 95% of cervical cancer cases are attributed to persistent infection with the human papillomavirus.[1] Literature indicates a significant treatment gap for patients with advanced, recurrent metastatic cancer, where the five-year survival rate stands merely at 16.8%.[2] In recent years, immunotherapy has emerged as a crucial component in the clinical management of cervical cancer: Programmed cell death protein 1 (PD-1)/programmed cell death ligand 1 (PD-L1) immune checkpoint inhibitors (ICIs) have been identified in most cases of cervical intraepithelial neoplasia (CIN) and cervical squamous cell carcinomas (CESCs), with notable PD-L1 expression.[3,4] Therapeutics targeting PD-1/PD-L1 exhibit promising prospects in cervical cancer treatment, although the precise mechanisms of this pathway in tumor metastasis remain largely unelucidated. Concurrently, clinical trials involving ipilimumab, a cytotoxic T-lymphocyte-associated protein 4 inhibitor, are underway for cervical cancer.[5,6] Thus, exploring effective diagnostic biomarkers and therapeutic targets for cervical cancer is of paramount importance.[7]

Tumor mutation burden (TMB), defined as the number of somatic mutations per megabase in the tumor genome, excluding germline mutations, primarily comprises non-synonymous mutations (nucleotide variations causing amino acid changes).[8,9] Theoretically, a higher TMB correlates with greater neoantigen production recognized by T cells. Extensive research suggests that higher TMB in tumor tissues, indicating an increased neoantigen load, enhances the efficacy of PD-1/PD-L1 inhibitors.[10] In patients with non-small cell lung cancer (NSCLC), tumor mutation load (ML) is categorized into low (<25%), medium (25–75%), and high (>75%) groups. Results indicate improved overall survival (OS), progression-free survival, and objective response rate in patients with high tumor ML.[11] For certain tumors, especially those with high TMB, such as melanoma and lung cancer, a higher TMB correlates with a greater neoantigen load.[12,13] These neoantigens can increase T cell content,[14] thereby eliciting anti-tumor immune responses. ICIs, by inhibiting checkpoint molecules like PD-1/PD-L1 and cytotoxic T-lymphocyte-associated protein 4, enhance the activity of anti-tumor T cells and help evade tumor immune responses.[15] TMB serves as a quantifiable metric for assessing tumor mutational load in therapeutic strategies. Clinical data extensively demonstrate that tumors with higher neoantigen loads or high TMB are more likely to derive clinical benefits from immunosuppressant treatments.[16]

Leveraging the immune system through immune checkpoint inhibition has significantly expanded treatment options for advanced cancers. Scholars using The Cancer Genome Atlas (TCGA) data from 5,722 tumor samples across 21 cancers have studied the correlation between immune cell status and tumor genetics,[17] including TMB, copy number alteration load, mutational allele tumor heterogeneity, and specific mutational signature types.[18] Among all genetic variables, mutational signatures associated with DNA repair defects and *AID*/*APOBEC* gene activity exhibited the strongest positive correlation with immune parameters.[17] Although TMB exhibits a bimodal or multimodal distribution in colorectal, gastric, and endometrial cancers, its levels are unrelated to or negatively correlated with key immune parameters across most cancer types. TMB typically shows a unimodal distribution in most other cancer types, including NSCLC and melanoma.[19] In summary, this study aims to reveal specific geno-immunological associations in major cancer types and suggests further exploration of mutation markers

as candidates for predictive response beyond TMB.

The mutation types considered for TMB assessment can vary across assays. These may include insertions and deletions, synonymous and non-synonymous base substitutions, and single nucleotide variants.[20] Retrospective analyses have observed that TMB assessments often only encompass missense mutations,[21] excluding insertions, deletions, and other variations, whereas targeted studies have included these variants, particularly because patients with mismatch repair deficiencies frequently present with high TMB.[22] Although TMB can predict the efficacy of immune checkpoint therapy and prognosis, TMB levels vary significantly across tumor types, and not all tumors exhibit high TMB. Previous studies have shown inconsistent TMB levels across different tumor types, such as the highest in melanoma, followed by NSCLC and other squamous cell carcinomas, while leukemias and pediatric tumors display low TMB levels, and breast, kidney, and ovarian cancers show intermediate levels, suggesting the need for distinct high- and low-TMB categorization standards for different cancers.[23,24] In recent years, TMB has played a crucial role in evaluating the efficacy of immunotherapy in lung cancer, but the specific mechanisms by which it regulates changes in the tumor microenvironment remain poorly understood. Recent efforts to utilize TMB for CESC prognosis have yielded inconsistent results, often failing to account for the intricate interplay between somatic mutations and the specific immune microenvironment. Therefore, there is a critical need to move beyond simple mutation counting and identify specific TMB-associated molecular signatures that can better stratify patient risk and therapeutic response. This article uses bioinformatics data to summarize and analyze the impact of TMB on CESC prognosis and further explores the relationship between TMB and immune cell infiltration.

A comprehensive analysis of the data reveals intricate links between TMB levels and the CESC immune landscape. It is evident that a higher TMB correlates with increased immune cell infiltration, which could enhance the effectiveness of immunotherapies. This finding underscores the importance of considering TMB as a pivotal factor in tailoring cervical cancer treatments, particularly in the context of immunotherapy. Moreover, the study aims to highlight the necessity to customize TMB assessment parameters across different tumor types. The variability in TMB across cancers demands a more nuanced approach to categorizing TMB. This could lead to more precise and effective treatments, especially in personalized medicine. In summary, the evolving understanding of TMB and its relation to the immune microenvironment in cervical cancer offers new avenues for research and clinical application. By focusing on TMB and its interplay with immune responses, we can potentially improve prognosis and therapeutic outcomes for cervical cancer patients.

2. Materials and methods

2.1. Acquisition of multi-omics data resources

The data utilized in this study are sourced from TCGA database, encompassing CESC mutation data, transcriptome profiles, and clinical information such as age, gender, American Joint Committee on Cancer TNM staging, pathological staging, tumor staging, and survival outcomes. Somatic mutation statistics were visualized using the "maftools" package in R (version 4.3.1). Patient transcriptome data were also downloaded from the TCGA database. To ensure the consistency and reliability of the study, strict inclusion and exclusion criteria were applied to the TCGA–CESC cohort. Inclusion criteria were: (i) samples with a confirmed pathological diagnosis of CESC; (ii) the availability of both somatic mutation data (MAF files) and transcriptomic profiles (RNA sequencing); and (iii) complete fundamental clinical information, including age, tumor stage, and survival status. Exclusion criteria were: (i) samples from recurrent or metastatic sites (only primary tumor samples with TCGA barcodes ending in "01A" were retained); (ii) patients with a follow-up period of less than 10 days to mitigate the impact of non-cancer-related perioperative mortality; and (iii) samples with significant missing data in key variables. After applying these filters, 308 samples were used for the whole-genome mutational landscape analysis, while 305 samples with paired mutation and clinical data were used for TMB-related calculations. To validate the generalizability of the *PTGS2*-based prognostic model, an independent clinical cohort was obtained from the Genomic Data Commons (GDC) database, specifically the CGCI–HTMCP–CC project. Transcriptomic data and corresponding clinical metadata (including the International Federation of Gynecology and Obstetrics stage and survival outcomes) were downloaded and processed.

2.2. Correlation analysis of tumor mutational burden with prognosis

Initially, germline mutations annotated in the dbSNP and ExAC databases were filtered out. For transcriptomic data, raw counts were converted to transcripts per million (TPM) values, which are more suitable for cross-sample comparisons and immune infiltration estimation than reads per kilobase million or fragments per kilobase million. To reduce data skewness and stabilize variance for downstream linear modeling, a $\log_2(\text{TPM} + 1)$ transformation was applied. Genes with extremely low expression (average count < 1 across all samples) were filtered out to minimize

biological noise. For TMB calculation, somatic mutation data were processed using the "maftools" package. TMB was quantified as the total number of non-synonymous mutations (including missense, nonsense, and splice site mutations) divided by the total length of the human exome (assumed to be 38 Mb). Subsequently, TMB for each sample was defined and calculated as the total number of coding variants divided by the length of exons (38 million), where detected variants were considered as frame-shift deletions, in-frame deletions, frame-shift insertions, in-frame insertions, missense mutations, nonsense mutations, splice site mutations, and silent mutations. Based on the median TMB value, patients were divided into high- and low-TMB groups. To ensure the biological relevance of our stratification, the threshold for defining "High" versus "Low" TMB was determined using two complementary approaches. While the median value was initially used for preliminary grouping, we subsequently used the maximally selected rank statistics (maxstat) in the survminer R package. This outcome-oriented approach identifies the "optimal" cutoff by maximizing the log-rank statistic, thereby providing a more biologically meaningful division based on patient survival hazard. Kaplan–Meier survival analysis and the log-rank test were used to assess differences in survival between high- and low-TMB groups. To improve accuracy in the Kaplan–Meier survival analysis, samples with survival times of less than 10 days were excluded. Additionally, the correlation between TMB distribution and clinical variables (American Joint Committee on Cancer TNM staging, tumor staging) was assessed using the Kruskal–Wallis test. Differential expression genes (DEGs) between the two TMB groups, high and low, were identified using the "limma" package in R[25] considering |log fold change (FC)| > 1.5 and false discovery rate < 0.05. Heatmaps for visualizing the differences were generated using the "pheatmap" package. The ClusterProfiler package was used for Gene Ontology (GO) and Kyoto Encyclopedia of Genes and Genomes (KEGG) analyses (q < 0.05), and Gene Set Enrichment Analysis (GSEA) was performed using TMB levels as a phenotype, with a false discovery rate < 0.3.

2.3. Identification of prognostic genes

Univariate Cox analysis was conducted using the "survival" package to select differentially expressed prognostic genes with p < 0.05. This was followed by a multivariate Cox analysis using stepwise regression to further identify independent risk factors. TMB related score (TMBRS) was calculated as Σ(βi×expi), where βi could be derived from multivariate Cox analysis. Receiver operating characteristic curves were plotted to assess the predictive capacity of TMBRS via the "timeROC" package, and Kaplan–Meier analysis employing the log-rank test was completed using the "survival" package.

2.4. Tumor Immune Estimation Resource

Tumor Immune Estimation Resource (TIMER) is an online database for comprehensive analysis of tumor immune cell infiltration (http://cistrome.dfci.harvard.edu/TIMER/). In this study, TIMER was used to compare the abundance of six immune cell subtypes (B cells, $CD4^+$ T cells, $CD8^+$ T cells, dendritic cells, macrophages, and neutrophils) between low- and high-TMB groups. Kaplan–Meier survival curves depicting the relationship between the abundance of 22 immune cells and survival risks were obtained in TIMER 2.0 (http://timer.cistrome.org/), along with corresponding hazard ratios and p-values. Scatter plots were used to describe the positive and negative correlations between risk gene expression and immune cell content.

2.5. Cell-type Identification by Estimating Relative Subsets of RNA Transcripts

Cell-type Identification by Estimating Relative Subsets of RNA Transcripts (CIBERSORT) is a novel computational algorithm for characterizing the composition of cell subgroups using RNA sequencing or microarray data from a large number of samples. CIBERSORT's accuracy is well-validated by immunohistochemistry or flow cytometry. It was used to calculate the proportions of 22 immune cell subtypes in each sample, with the ratios summing to 1. A total of 1,000 permutations were conducted, and samples with p < 0.05 were retained to enhance the accuracy of the estimates. Heatmaps were constructed to display the distribution of immune cell proportions, and violin plots were used to visualize the differential distributions of cells between groups with high and low TMB levels.

2.6. Statistical analysis

To address potential batch effects and technical variations inherent in large-scale multi-center genomic data, we used GDC-harmonized data, processed with a unified bioinformatics pipeline. During differential expression analysis, the limma package's internal normalization procedures were employed to correct for systematic technical biases. Continuous variables were compared using the Wilcoxon rank-sum test (two groups) or the Kruskal–Wallis test (multiple groups). Survival analysis was conducted using the log-rank test to compare Kaplan–Meier curves, and multivariate Cox regression was performed using a stepwise approach to identify independent prognostic indicators while adjusting for clinical covariates. Statistical significance was defined as p-value < 0.05.

2.7. External validation and model robustness

The predictive accuracy of the TMBRS in the external cohort was evaluated using time-dependent ROC curves and the Concordance Index (C-index). To assess the model's stability, a bootstrap resampling procedure (n = 1,000) was used to estimate the distribution of the C-index. The non-linear relationship between *PTGS2* expression and patient hazard rates was explored using a restricted cubic spline Cox model with three knots. Furthermore, the optimal threshold for risk stratification in the validation cohort was determined using the maximally selected rank statistics (maxstat) to achieve the greatest separation of survival curves. Correlation analysis between *PTGS2* and immune programs was performed using Spearman's rank correlation based on established marker-based immune signatures. Statistical significance was defined as p-value < 0.05.

3. Results

3.1. Whole-genome mutational landscape of cervical squamous cell carcinoma

Somatic mutation data from 308 CESC patients were analyzed from the TCGA database, along with their clinical information, as summarized in Table 1. The cohort included 225 (73.1%) patients aged ≤55 years and 83 (26.9%) patients aged >55 years. Using the "maftools" package in R, these mutations were grouped and visualized in a boxplot, with each group distinguished by a different color (Figure 1). The most common mutation type identified was missense mutations (Figure 1A); single nucleotide polymorphisms occurred more frequently than deletions or insertions (Figure 1B), with C>T transitions being the most prevalent single nucleotide variant in CESC (Figure 1C). The mutation categories are depicted in a boxplot (Figure 1E). The top 10 mutated genes included *TTN* (29%), *PIK3CA* (27%), *KMT2C* (18%), *MUC4* (18%), *MUC16* (16%), *KMT2D* (13%), *DMD* (12%), *FBXW7* (12%), *FLG* (12%), and *EP300* (11%) (Figure 1F and 1G).

3.2. Tumor mutational burden and its association with clinical staging

We calculated the TMB per million bases for 305 samples and used the median value as a threshold to divide them into high- and low-TMB groups. Kaplan–Meier survival curves revealed no direct correlation between TMB levels and overall survival of patients (p = 0.720) (Figure 2A). Furthermore, the results suggested a marginal association between TMB levels and tumor T staging (p = 0.057; Figure 2D), although this did not reach statistical significance. No significant associations were observed between TMB levels and histopathological grade (p = 0.800, Figure 2C), M stage (p = 0.361, Figure 2E), or N stage (p = 0.950, Figure 2F). Additionally, TMB levels tended to increase with tumor progression (Figure 2**C–E**), underscoring the need for larger clinical studies to validate these findings.

Table 1. Clinical characteristics of samples from The Cancer Genome Atlas database

Variable	*n* (%)
Age (years)	
≤55	225 (73.1)
>55	83 (26.9)
Survival status	
Live	73 (23.7)
Death	235 (76.3)
Tumor T stage	
T1	143 (46.5)
T2	72 (23.4)
T3	21 (6.8)
T4	10 (3.2)
TX	62 (20.1)
Tumor M stage	
M0	117 (38.0)
M1	10 (3.2)
MX	181 (58.8)
Tumor N stage	
N0	135 (43.8)
N1	61 (19.8)
NX	112 (36.4)
Histopathological grade	
G1	19 (6.1)
G2	136 (44.2)
G3	120 (39.0)
G4	1 (0.3)
GX	32 (10.4)

3.3. Analysis of differentially expressed genes in two tumor mutation burden groups

Forty DEGs were analyzed using R and displayed in a heatmap (Figure 3A). Subsequently, KEGG pathway analysis indicated that TMB-related signals were involved in several pathways, mainly including cytokine–cytokine receptor interaction and bile secretion (Figure 3B and Table 2). Additionally, GSEA of TMB-associated gene

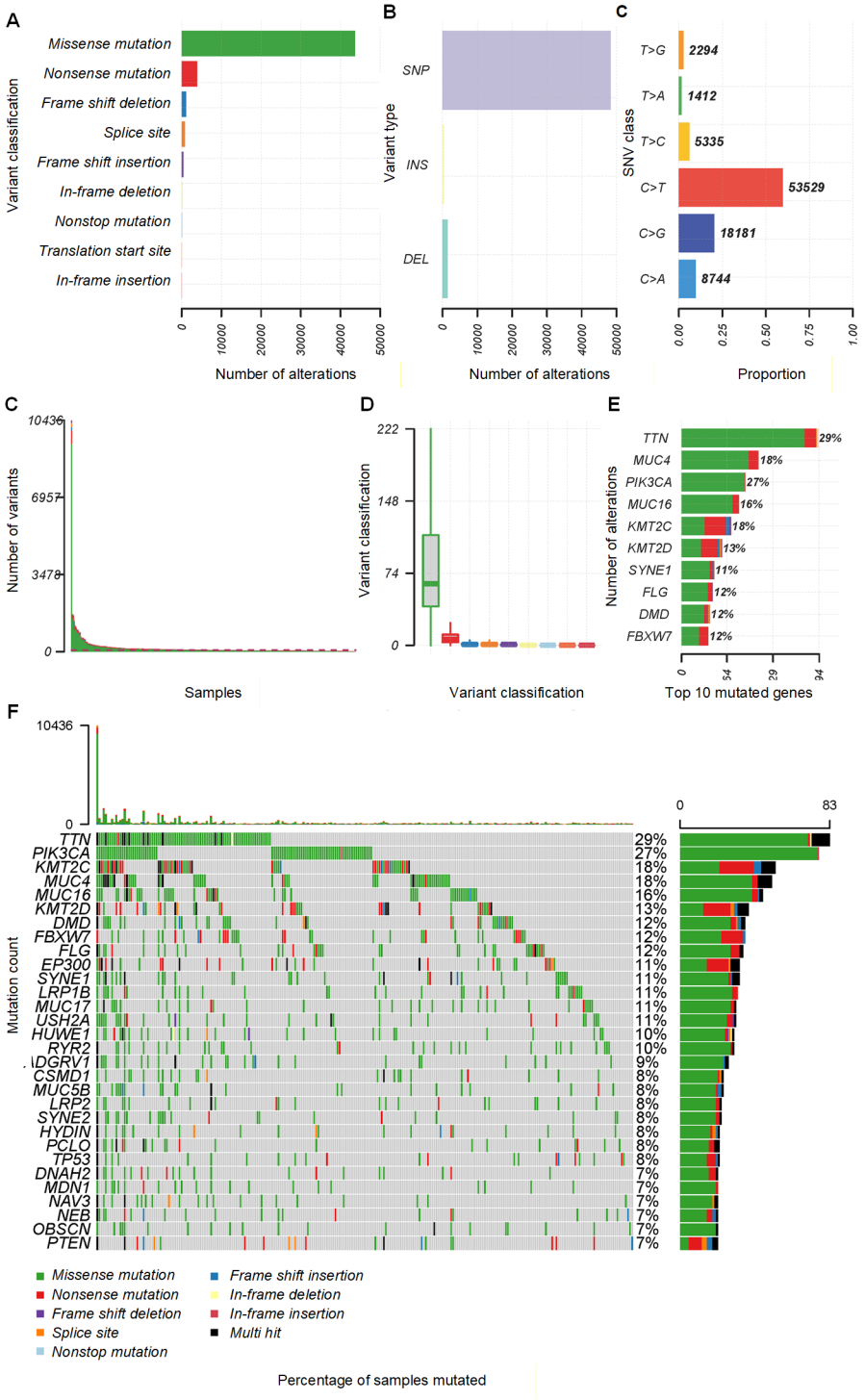

Figure 1. Summary of mutational analysis in CESC samples. (A–C) Statistical analysis of mutation types by category, with missense mutations being predominant, SNPs more frequent than deletions or insertions, and C>T being the most common type of SNV. (A) Variant classification. (B) Variant type. (C) Single nucleotide variant class. (D–E) Illustration of tumor mutation burden in specific samples. (D) Variants per sample. (E) Variant classification summary. (F) Top 10 mutated genes in CESC. (G) Overview of mutations in CESC samples, with each gene mutation in each sample displayed in a waterfall plot, where different colors with specific annotations at the bottom represent different mutation types. The bar graph above the legend shows the number of mutation burdens.

Abbreviations: CESC: Cervical squamous cell carcinoma; SNP: Single nucleotide polymorphism; SNV: Single nucleotide variant.

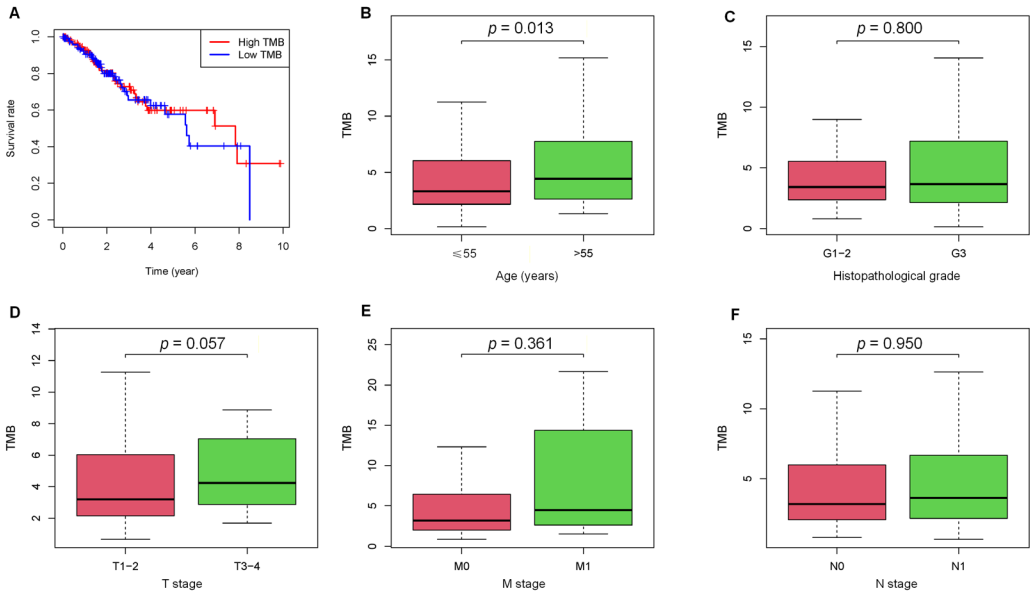

Figure 2. Prognostic analysis of tumor mutational burden (TMB) and its correlation with clinical risk features. (A) Higher TMB is associated with better overall survival (OS) outcomes ($p = 0.720$). (B) Boxplot showing patients over 55 years of age had higher TMB values than those under 55 ($p = 0.013$). (C–F) Higher TMB levels were associated with advanced (D) tumor T staging ($p = 0.057$), with no significant differences in (C) histopathological stage or (E) M and (F) N stages ($p > 0.05$).

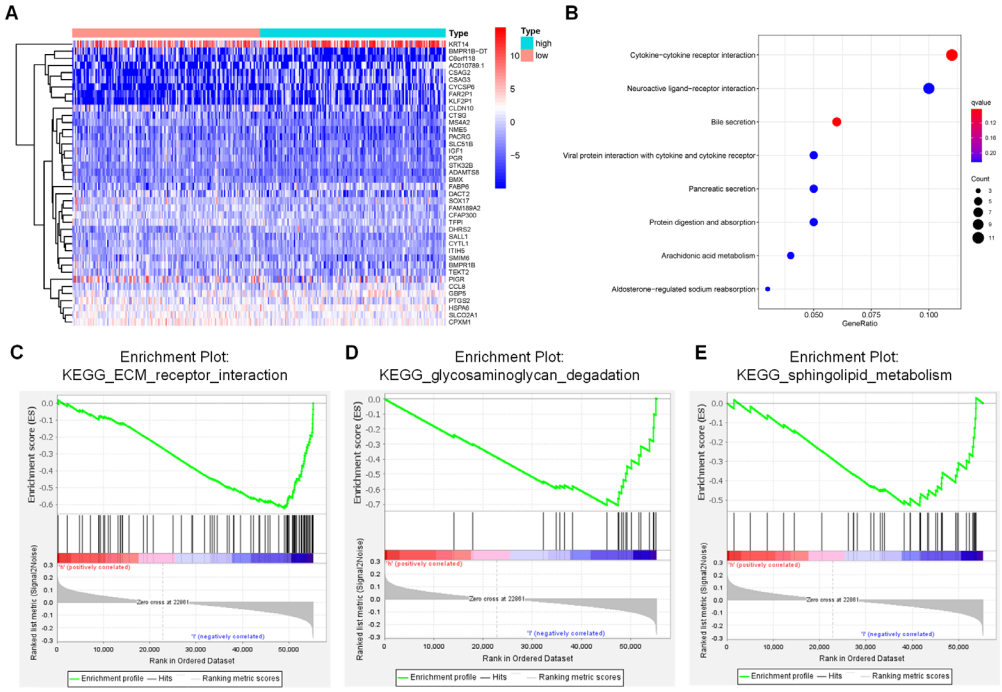

Figure 3. Comparative analysis of differentially expressed genes between low- and high-TMB groups and enrichment pathway analysis. (A) Heatmap displaying the expression of 40 differentially expressed genes in low- and high-TMB groups, where pink and blue represent low- and high-TMB groups, and red and blue indicate high and low gene expression, respectively. (B) KEGG pathway analysis shows that these genes are mainly involved in cytokine–cytokine receptor interaction, bile secretion, and other pathways. (C–E) GSEA enrichment analysis indicates that extracellular matrix (ECM) receptor interaction, glycosaminoglycan degradation, and sphingolipid metabolism are related to lower TMB levels.

Abbreviations: CESC: Cervical squamous cell carcinoma; GSEA: Gene Set Enrichment Analysis; KEGG: Kyoto Encyclopedia of Genes and Genomes; TMB: Tumor mutational burden.

sets showed that extracellular matrix receptor interaction, glycosaminoglycan degradation, and sphingolipid metabolism were associated with lower TMB levels (Figure 3C–F). GO enrichment analysis revealed that in biological pathways, these genes were mainly involved in processes like epithelial cell branching morphogenesis and tube formation; in molecular functions, they were related to activities such as peptidase regulator activity and glycosaminoglycan binding; and in cellular components, they were predominantly found in motile cilia and extracellular matrix collagen (Figure 4A and 4B).

Table 2. Kyoto Encyclopedia of Genes and Genomes pathway analysis of differential genes

Pathway	Gene ratio	*p*-value	*p*.adjust	*q*-value	Gene ID
Bile secretion	6/100	0.0008187	0.086304	0.083660	*SLC22A1/UGT2B7/UGT1A7/SLC51B/SCTR/ATP1B2*
Cytokine–cytokine receptor interaction	11/100	0.0009752	0.086304	0.083660	*PPBP/CCL8/CCL19/CXCL2/TNFSF18/INHA/IFNK/CCL25/NGF/IL9R/BMPR1B*
Arachidonic acid metabolism	4/100	0.0066494	0.230943	0.223870	*PLA2G10/PTGS2/PTGIS/CYP4F2*
Viral protein interaction with cytokine and cytokine receptor	5/100	0.0077264	0.230943	0.223870	*PPBP/CCL8/CCL19/CXCL2/CCL25*
Pancreatic secretion	5/100	0.0083849	0.230943	0.223870	*PRSS1/PRSS2/PLA2G10/SCTR/ATP1B2*
Protein digestion and absorption	5/100	0.0087284	0.230943	0.223870	PRSS1/DPP4/PRSS2/ATP1B2/COL2A1
Neuroactive ligand–receptor interaction	10/100	0.0091334	0.230943	0.223870	*PRSS1/RXFP1/PRSS2/ADRA2A/CTSG/TRH/ADRA1B/KISS1R/SCTR/SST*
Aldosterone-regulated sodium reabsorption	3/100	0.0104508	0.231223	0.224142	*FXYD4/ATP1B2/IGF1*

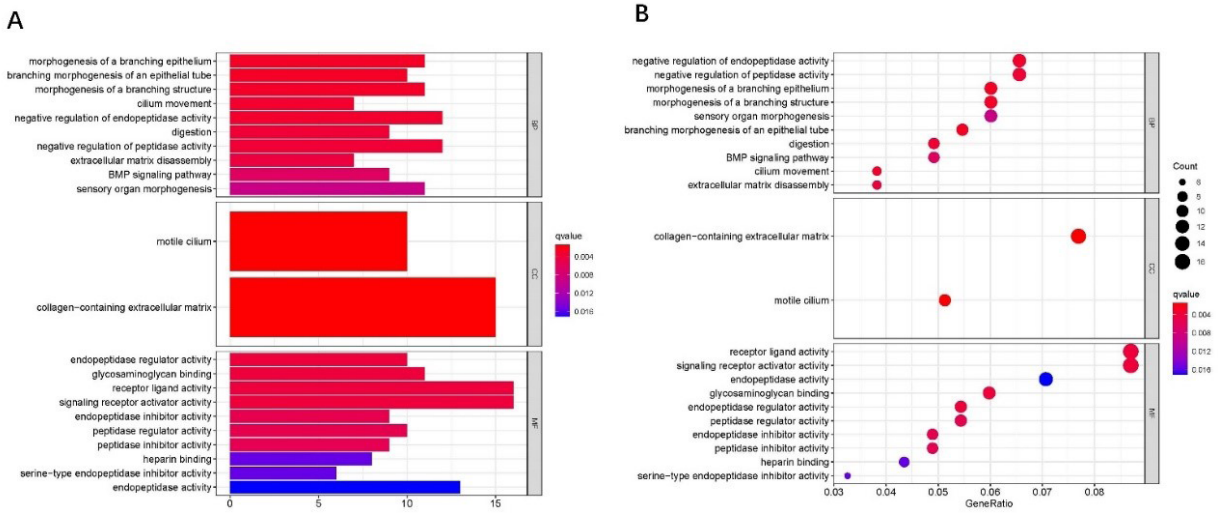

Figure 4. Gene Ontology (GO) enrichment analysis. The GO analysis indicates that, within biological pathways (BP), genes are predominantly involved in processes such as epithelial cell branching morphogenesis and epithelial tube formation. In terms of molecular functions (MF), they were associated with activities like peptidase regulator activity and glycosaminoglycan binding. For cellular components (CC), significant occurrences were noted in motile cilia and extracellular matrix collagen. (A) Bar plot. (B) Bubble plot.

Additionally, eight potential risk genes associated with variations in TMB were identified through univariate and multivariate Cox analyses (Table 3): cathepsin G gene (*CTSG*), prostaglandin-endoperoxide synthase 2 (*PTGS2*), bone morphogenetic protein receptor type 1B (*BMPR1B*), progesterone receptor (*PGR*), heat shock protein 70 kDa family member 6 (*HSPA6*), C-C motif chemokine ligand 8 (*CCL8*), fatty acid binding protein 6 (*FABP6*), and insulin-like growth factor 1 (*IGF1*). Notably, *PTGS2* showed a unique risk feature with a *p*-value of <0.05.

A multivariate Cox regression model based on *PTGS2* was used to construct a TMBRS as follows: TMBRS = 0.0239139 × PTGS2. Using the median value as a threshold, patients with CESC were categorized into high-risk and low-risk groups. Kaplan–Meier plots showed that patients in the high-risk group tended to have lower survival rates than those in the low-risk group, though this difference did not reach statistical significance in this cohort ($p = 0.199$; Figure 5A). The five-year ROC curve indicates moderate predictive accuracy with an area under the curve (AUC) of 0.696 (Figure 5B). While this demonstrates the preliminary utility of TMBRS for risk stratification, the results should be interpreted as an exploratory foundation for future clinical validation. The association between this gene's risk and survival warrants further investigation and validation in larger samples.

Table 3. Multifactorial Cox analysis of tumor mutational burden-related features in cervical squamous cell carcinoma patients

Genes	Hazard ratio	95% confidence interval lower	95% confidence interval upper	Cox *p*-value
CTSG	0.7976	0.4970	1.2798	0.3485205
PTGS2	1.0092	1.0012	1.0173	0.0239139
BMPR1B	1.0337	0.9708	1.1006	0.3013682
PGR	1.0201	0.9848	1.0568	0.2681945
HSPA6	1.0046	0.9985	1.0109	0.1416605
CCL8	0.9409	0.8617	1.0274	0.1743890
FABP6	0.9933	0.9691	1.0181	0.5927633
IGF1	1.0096	0.8365	1.2187	0.9203763

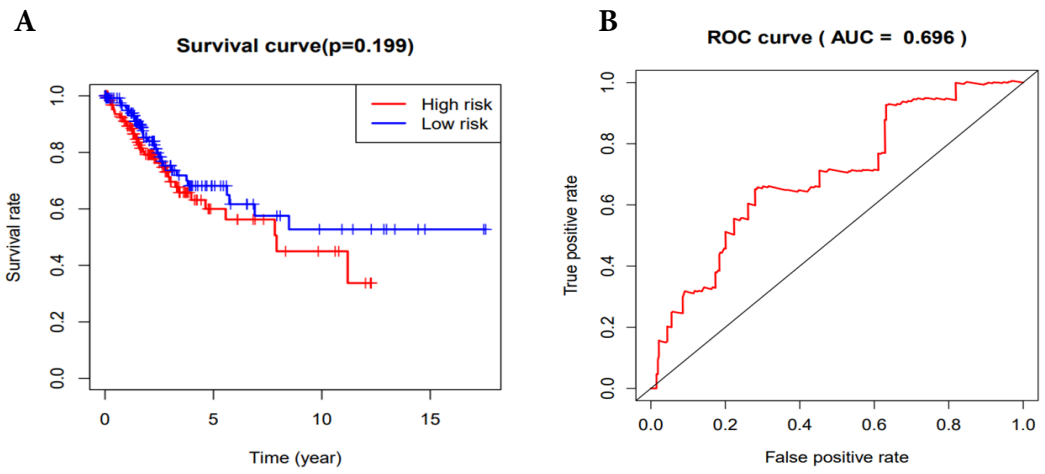

Figure 5. Tumor mutational burden risk model in CESC. (A) Kaplan–Meier analysis using the log-rank test indicates poorer overall survival in patients with a higher tumor mutation burden-related risk score ($p = 0.199$). (B) The ROC plot with an AUC of 0.696 demonstrates higher predictive accuracy of the model.
Abbreviations: AUC: Area under the curve; CESC: Cervical squamous cell carcinoma; ROC: Receiver operating characteristic.

3.4. Comparison of immune cell abundance in high- and low-tumor mutational burden groups

Using the CIBERSORT software and the R package, we analyzed differences in the immune profile between high- and low-TMB groups in CESC patients. After filtering out samples with $p > 0.05$, we obtained profiles for 22 immune cell types, as depicted in Figure 6A, where different colors represent different immune cell subtypes. These included various T cells (activated, central memory and effector memory $CD4^+$ and $CD8^+$ T cells, γδ T cells, regulatory T cells [Tregs], follicular helper T cells [Tfh], helper T cells [Th1, Th2, Th17]), B cells [activated, immature, and memory], and myeloid cells, such as macrophages, activated, plasma-like, and immature dendritic cells [DC], monocytes, mast cells, eosinophils, neutrophils, natural killer [NK] cells, NK T cells, and bone marrow mesenchymal stem cells). The Wilcoxon rank-sum test revealed that the infiltration levels of $CD8^+$ T cells ($p = 0.008$), activated memory $CD4^+$ T cells ($p = 0.031$), Tfh cells ($p = 0.003$), Tregs ($p = 0.024$), and M1 macrophages ($p = 0.005$) were higher in the high-TMB group compared to the low-TMB group. Additionally, an analysis of the GSEA database showed lower levels of NK cells, dendritic cells, and $CD4^+$ T cells in all patients, whereas levels of M1 macrophages, M2 macrophages, neutrophils, and $CD8^+$ T cells were higher (Figure 6B). Conversely, the infiltration level of M0 macrophages ($p = 0.055$) was higher in the low-TMB group compared to the high-TMB group (Figure 6C).

3.5. Relationship between immune cell abundance and prognosis

This study aimed to compare immune infiltration between high- and low-immune infiltration groups; patients were categorized based on the median content of each immune cell. The potential prognostic implications of immune cells were then explored using the TIMER 2.0 database. Kaplan–Meier plots (Figure 7) indicated that higher infiltration levels of activated memory $CD4^+$ T cells (hazard ratio [HR] = 0.666, $p = 0.00621$), memory B cells (HR = 0.747, $p = 0.0286$), γδ T cells (HR = 0.529, $p = 0.0133$), and $CD8^+$ T cells (HR = 0.651, $p = 0.000578$) correlated with lower risk and longer expected survival times. Conversely, higher neutrophil infiltration (HR = 1.23, $p = 0.0789$) was associated with a higher risk and shorter expected survival times (Table 4).

3.6. Comparative analysis of risk genes and immune cell relationships

To investigate the correlation between immune infiltration and *PTGS2* gene expression in patients with CESC, we focused on six immune cell types that showed significant differences between high- and low-TMB groups, as previously identified. Using the TIMER 2.0 database, scatter plots (Figure 8) were constructed. These plots revealed a negative correlation between *PTGS2* gene expression and the abundance of $CD8^+$ T cells and M1 macrophages. However, there was no significant association between *PTGS2* expression and other immune cells, including activated memory $CD4^+$ T cells, Tfh cells, Tregs, and M0 macrophages.

Furthermore, to explore *PTGS2* expression in CESC and other cancers, the TIMER 2.0 tool was used. Box plots (Figure 9A) showed that PTGS2 is highly expressed in esophageal cancer and head and neck squamous cell carcinoma, whereas it is expressed at lower levels in cancers such as bladder cancer, breast cancer, renal cell carcinoma, clear cell renal carcinoma, papillary renal cell carcinoma, hepatocellular carcinoma, lung adenocarcinoma, lung squamous carcinoma, prostate cancer, and endometrial cancer. Although the data for cervical cancer were not statistically significant due to limited normal cell data, previous studies have indicated an upregulation of COX-2

Table 4. Univariate Cox analysis of six major immune cells

Cells	Coefficient	Hazard ratio	95% confidence interval lower	95% confidence interval upper	*p*-value
B cell	−1.872	0.154	0.000	1,324.554	0.686
CD8 T cell	−4.799	0.008	0.000	0.961	0.048
CD4 T cell	−5.688	0.003	0.000	7.542	0.148
Macrophage	1.979	7.236	0.006	8,707.998	0.584
Neutrophil	−2.622	0.073	0.000	631.194	0.571
Dendritic cell	3.699	40.399	0.372	4,388.085	0.122

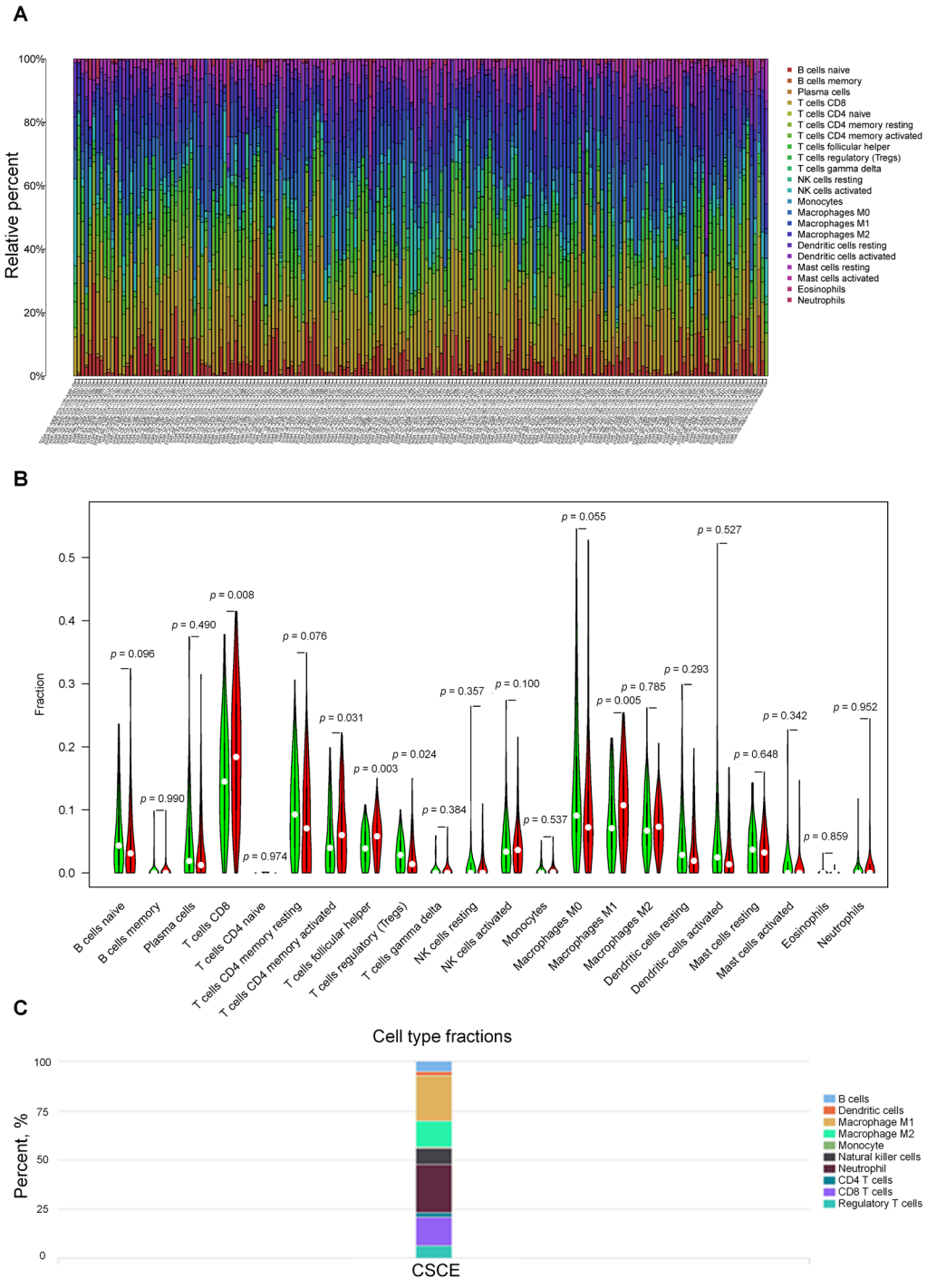

Figure 6. Summary of immune cell subtype estimates from the CIBERSORT algorithm. (A) Each bar graph shows the proportions of cells for each patient, with different colors indicating the 22 immune cell types. (B) Violin plots in green and red represent low- and high-TMB groups, respectively, showing higher infiltration levels of $CD8^+$ T cells, activated memory $CD4^+$ T cells, follicular helper T cells (Tfh), regulatory T cells (Tregs), and M1 macrophages in the high-TMB group. Conversely, M0 macrophages show higher infiltration in the low-TMB group. (C) Immune cell composition based on the GSEA algorithm, with natural killer cells, dendritic cells, and $CD4^+$ T cells showing lower infiltration levels, whereas M1 macrophages, M2 macrophages, neutrophils, and $CD8^+$ T cells show higher levels.

Abbreviations: CIBERSORT: Cell-type Identification by Estimating Relative Subsets of RNA Transcripts; GSEA: Gene Set Enrichment Analysis; TMB: Tumor mutational burden.

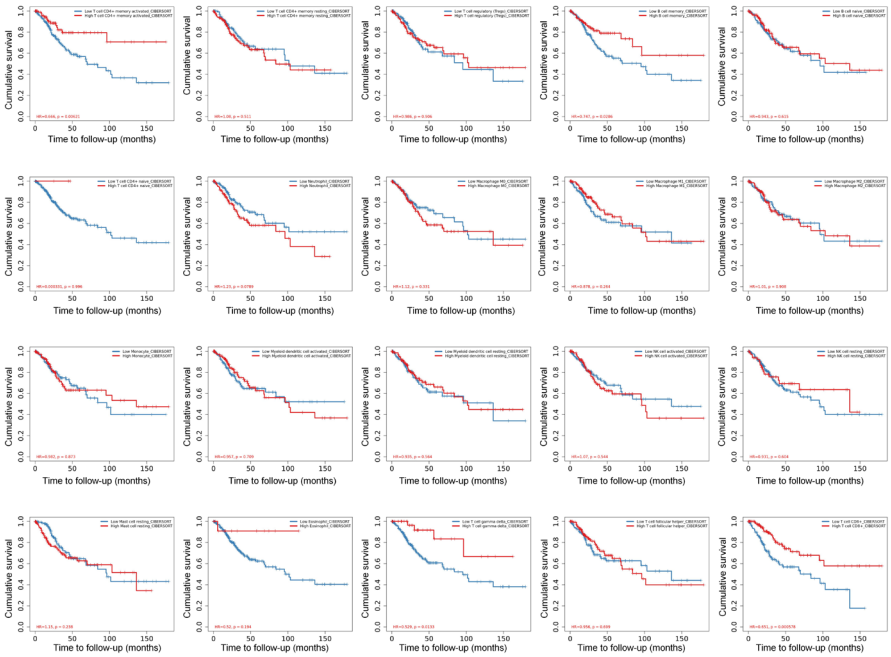

Figure 7. Relationship between immune cell abundance and survival risk based on Tumor Immune Estimation Resource 2.0. The figure illustrates that higher infiltration of activated memory CD4⁺ T cells, memory B cells, γδ T cells, and CD8+ T cells is associated with longer survival and lower risk, whereas higher infiltration of neutrophils is associated with shorter survival and increased risk.

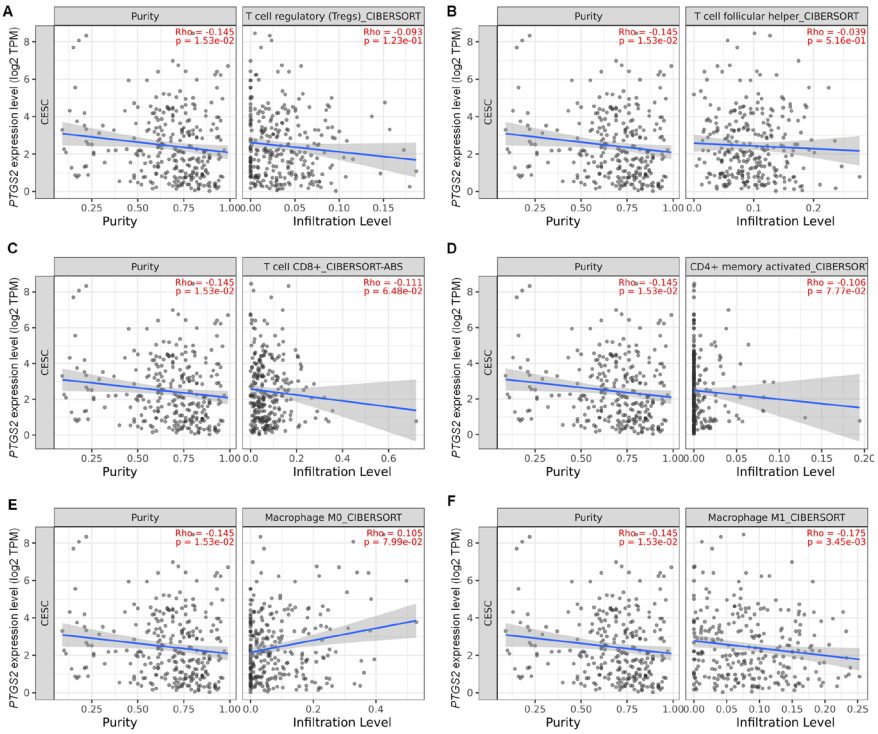

Figure 8. Correlation between *PTGS2* gene expression and immune cell abundance. The sub-figures (A–F) display the relationship between *PTGS2* gene expression and (A) regulatory T cells, (B) follicular helper T cells, (C) CD8+ T cells, (D) activated memory CD4⁺ T cells, (E) M0 macrophages, and (F) M1 macrophages, respectively. The scatter plots particularly highlight the negative correlation between *PTGS2* expression and the abundance of CD8+ T cells and M1 macrophages.

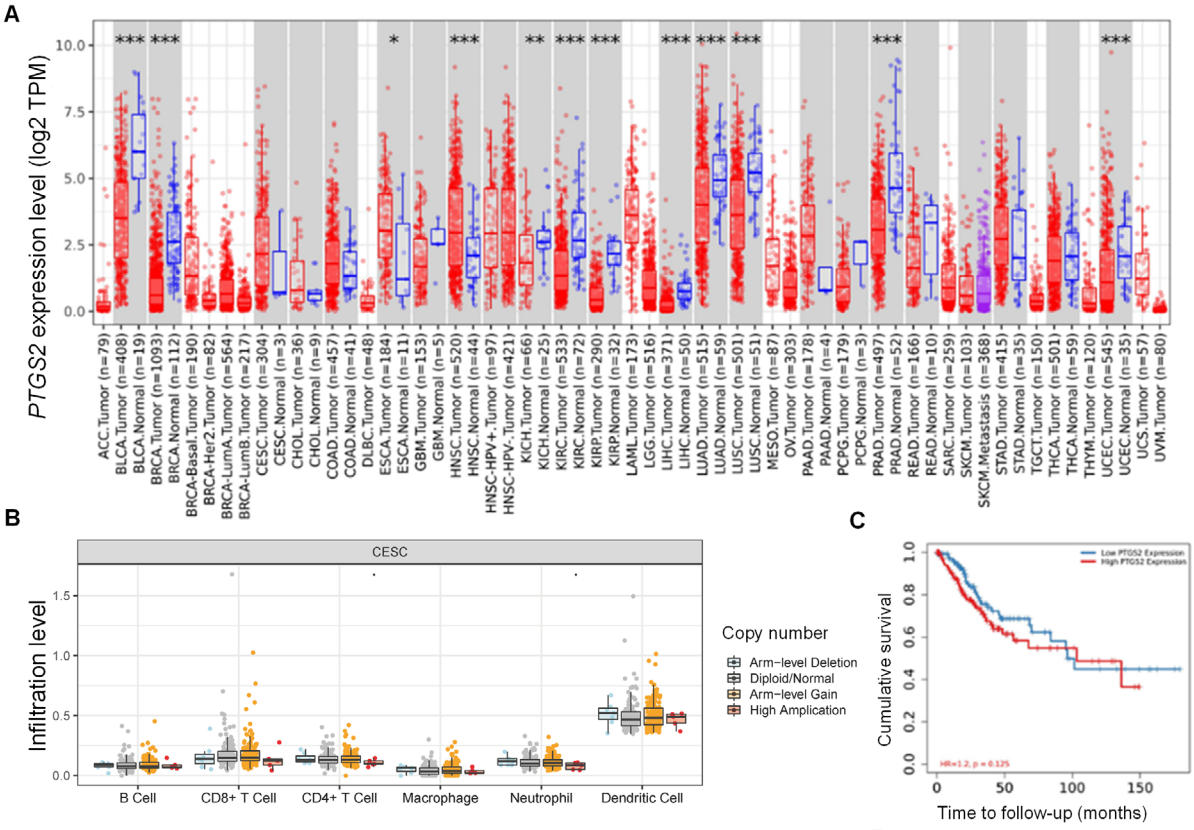

Figure 9. *PTGS2* gene expression mutations and their relationship with cancer. (A) The expression of the *PTGS2* gene in various cancers, indicating upregulation or downregulation. (B) Relationship between *PTGS2* gene copy number variations and the infiltration levels of six types of immune cells, where blue represents a loss of one copy, gray indicates no change in copy number, yellow signifies gaining one copy, and red indicates gaining two copies. (C) The relationship between *PTGS2* gene expression and survival rates. *$p < 0.05$, **$p < 0.01$, and ***$p < 0.001$.

expression in cervical cancer tissues. Analysis of *PTGS2* gene copy number variations and immune cell abundance (Figure 9B) indicated that, compared to other groups, having two copies of the gene is associated with a reduced abundance of $CD4^+$ T cells and neutrophils.

3.7. External validation of the *PTGS2*-based prognostic model and immune landscape

To verify the robustness and clinical applicability of our findings, we conducted external validation using the GDC project CGCI–HTMCP–CC (an independent cervical cancer cohort).

3.7.1. Robustness of PTGS2 as a clinical and prognostic marker

In the external cohort, *PTGS2* expression remained a significant indicator of tumor progression and patient outcome. Survival analysis demonstrated that the prognostic value of TMBRS, primarily driven by *PTGS2* expression, was consistent with our TCGA findings, showing a clear separation in survival probability between high- and low-risk groups (Figure 10A and 10I). Furthermore, *PTGS2* expression was significantly associated with external International Federation of Gynecology and Obstetrics staging, confirming its role as a marker for advanced disease (Figure 10B).

3.7.2. Predictive accuracy and risk stratification

The prognostic efficacy of the model was further quantified using several statistical approaches: Cox regression confirmed that *PTGS2* and the derived TMBRS are independent risk factors after adjusting for clinical covariates (Figure 10E). The time-dependent ROC curve at two years yielded a high AUC, and the bootstrap distribution of the C-index (n = 1,000) centered around a robust predictive value, indicating the model's high precision in an independent setting (Figure 10J and 10L). A restricted cubic spline model visualized the association between *PTGS2* expression and hazard rates, highlighting a potential nonlinear increase in risk with increasing

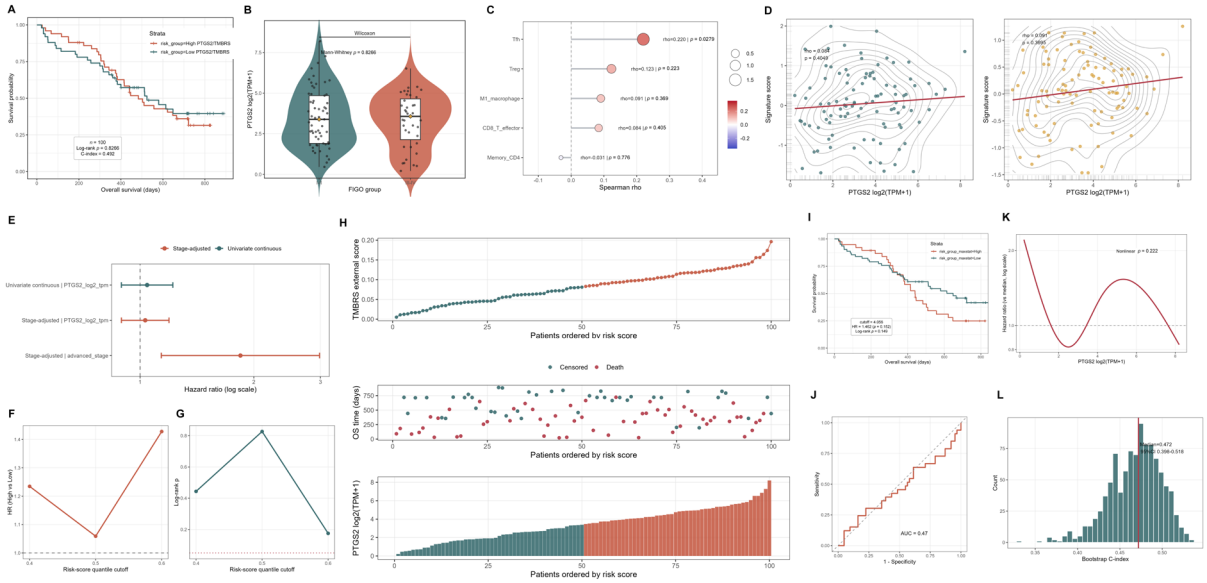

Figure 10. External validation of the *PTGS2*-based prognostic model and immune landscape in independent cohorts. (A) Kaplan–Meier curves showing overall survival (OS) in the CGCI–HTMCP–CC external validation cohort, stratified by the TMBRS model. (B) Violin plots illustrating the differential expression of *PTGS2* mRNA across various International Federation of Gynecology and Obstetrics clinical stages in the validation dataset. (C) Correlation heatmap representing the Spearman coefficients between *PTGS2* expression and diverse immune signatures/programs. (D) Scatter plots with density contours highlighting the significant associations of *PTGS2* expression with $CD8^+$ T effector cells and M1 macrophage infiltration signatures. (E) Forest plot displaying the Cox regression effect sizes (hazard ratio and 95% confidence intervals) for *PTGS2* and TMBRS across unadjusted and adjusted models. (F–G) Sensitivity analysis of TMBRS cutoff values illustrating the trends of hazard ratios and *p*-values to identify the optimal threshold for risk stratification. (H) Distribution of risk scores (top), survival status of individual patients (middle), and the corresponding *PTGS2* expression pattern (bottom) in the validation cohort. (I) Survival analysis employing the maximally selected rank statistics (maxstat) to determine the optimal *PTGS2* expression cutoff for patient prognosis. (J) Time-dependent receiver operating characteristic curve analysis of the model's predictive performance for two-year survival. (K) Restricted cubic spline analysis depicting the non-linear relationship between *PTGS2* expression levels and the hazard of mortality. (L) Distribution of the Concordance Index (C-index) derived from bootstrap resampling (n = 1,000) to evaluate the stability and accuracy of the prognostic model.

expression (Figure 10K).

3.7.3. Validation of the immune infiltration landscape

Crucially, the external data reinforced the interplay between *PTGS2* and the tumor immune microenvironment identified in our initial analysis. The correlation landscape linking *PTGS2* to various immune signatures confirmed a significant relationship with T cell and macrophage programs (Figure 10C). Specifically, scatter plots in the validation cohort highlighted the strong associations between PTGS2 levels and both $CD8^+$ T effector cells and M1 macrophage infiltration (Figure 10D). These results substantiate our conclusion that *PTGS2* expression is intrinsically linked to diminished immune recognition and poor prognosis in CESC.

4. Discussion

Cervical cancer remains one of the most common malignant tumors in gynecology. Despite significant improvements in early screening, resulting in a declining incidence rate, cervical cancer continues to be a major global health issue.[26] Since 2016, ICIs have shown promising results in the immunotherapy of advanced CESC.[27] However, only a small subset of CESC patients benefit from this treatment, leading many studies to focus on identifying predictive biomarkers for immunotherapy. In our current study, we found that mutations in *TTN* (29%) and *PIK3CA* (27%) were particularly prevalent in CESC. Mutations in *PIK3CA* lead to increased expression of the p110α protein,[28] a critical molecule in the phosphoinositide 3-kinase-protein kinase B signaling pathway, which is associated with cell survival and activation of anti-apoptotic signals. Wright *et al.*[29] investigated 1,250 known tumor mutation genes in 80 cervical cancer cases and found the highest mutation rate in *PIK3CA* (31.3%), with no significant difference between squamous and adenocarcinomas. *PIK3CA* mutations were associated with shorter survival. Other studies[30] suggest that overexpression of p110α protein could be a pathogenic factor for cervical precancerous lesions and cervical cancer. Furthermore, gynecological malignancies with *PIK3CA* mutations respond better to *PIK3CA* pathway inhibitors,[31] making *PIK3CA* mutation status a potential predictive marker for treatment efficacy. The *TTN* gene encodes titin,

and due to its long sequence, any mutation may disrupt titin function, leading to abnormal muscle fiber growth.[32] In cervical cancer, *TTN*-antisense RNA 1, driven by *TTN* mutations, promotes cell growth and invasion and inhibits apoptosis. High levels of *TTN*-antisense RNA 1 are associated with shorter progression-free survival.[33]

Higher TMB levels may indicate greater suitability for ICI treatment. Starting with treatments for advanced melanoma and NSCLC, TMB has emerged as a novel prognostic biomarker for ICI therapy, recently found to be applicable in breast cancer[34] and other malignancies. Samstein *et al.*[35] discovered that high-TMB patients undergoing ICI therapy had better OS. In our study, CESC patients with high TMB had better survival than those with low TMB, although this trend reversed after five years, possibly due to the generally older age of high-TMB patients. High TMB levels may also induce immune recognition and improve prognosis. The level of TMB was associated with histological grade and T stage and was positively correlated with M stage. However, larger clinical studies are needed to validate these results. These findings suggest that TMB levels increase with CESC progression, prompting us to explore the potential relationship between TMB-differential genes and immune infiltration to identify additional prognostic biomarkers for CESC.

Higher abundance of activated $CD4^+$ memory and $CD8^+$ T cells correlates with longer OS.[36] In recent years, immune infiltration in tumor immunotherapy has garnered increasing attention.[37] Techniques assessing $CD8^+$ and $CD3^+$ cells in tumor centers and immune infiltration are being utilized clinically.[38] A 2014 study identified $CD8^+$ T cells as a key factor in tumor immunotherapy, with their effect dependent on the composition of accompanying inflammatory cells, including macrophages, B cells, and CD4 tumor-infiltrating lymphocytes.[39] A 2016 study found high levels of $CD4^+$ and $CD8^+$ T cell infiltration in triple-negative breast cancer correlated with better clinical outcomes.[40] Previous research indicates that Tregs can suppress the proliferation of $CD4^+$ T cells and the secretion of interleukin-2.[41] Sato *et al.*[42] found that improving tumor-specific $CD8^+$ T cells and reducing Tregs effectively enhances cancer prognosis. Our study compared the differential abundance of immune cells in high- and low-TMB groups through violin plots, with $CD8^+$ T cells, activated memory $CD4^+$ T cells, Tfh cells, Tregs, and M1 macrophages showing higher infiltration in the high-TMB group. High infiltration levels of activated memory $CD4^+$ T cells (HR = 0.666, $p = 0.00621$), memory B cells (HR = 0.747, $p = 0.0286$), γδ T cells (HR = 0.529, $p = 0.0133$), and $CD8^+$ T cells (HR = 0.651, $p = 0.000578$) correlated with lower risk and longer survival times. The abundance of these immune cells, particularly activated $CD4^+$ memory and $CD8^+$ T cells, indicates higher TMB levels and correlates with longer expected survival and reduced risk.[43] These immune cells, particularly activated $CD4^+$ memory and $CD8^+$ T cells, can serve as prognostic indicators for CESC. While TMB holds promise as a biomarker, several issues remain, including the definition of high TMB across different tumor types, the optimal strategy for calculating TMB, which includes laboratory techniques, the number of regions of genes to be included, methods for screening germline variations, and other bioinformatics approaches. Overall, TMB is a promising biomarker with the potential to drive significant breakthroughs in cancer detection and treatment.

Compared with previously published CESC TMB analyses, which often categorized patients based solely on median TMB values, our integrated TMBRS model, validated in external cohorts (CGCI–HTMCP–CC), demonstrates enhanced predictive accuracy (AUC = 0.696). Previous studies have noted that TMB levels in gynecological malignancies are moderate and may not independently predict long-term survival. Our data refine this understanding by showing that the prognostic impact of TMB is mediated through specific immune-related genes and infiltration patterns, particularly involving $CD8^+$ T cells and M1 macrophages. By incorporating these biological variables, our model provides a more robust framework for personalized immunotherapy strategies than traditional TMB-only assessments.

Several limitations of this study should be acknowledged. First, the predictive utility of the current TMBRS model remains moderate (AUC < 0.70). This limitation likely stems from the inherent biological complexity of cervical cancer and the relatively modest sample size of the primary cohort. Notably, our prognostic model (TMBRS) is primarily based on *PTGS2* expression profiles. While *PTGS2* emerged as a distinctive independent risk feature in our analysis, relying on a single-gene signature may limit the overall robustness and clinical applicability of the model compared to more comprehensive multi-gene panels. Therefore, our model should be viewed as a proof-of-concept demonstrating the link between mutational burden and the immune microenvironment, rather than a finalized tool for clinical decision-making. Future studies incorporating additional variables, such as human papillomavirus viral load, specific epigenetic markers, or a broader array of TMB-related risk genes, may be needed to enhance the model's predictive power and reliability. Moreover, the lack of statistical significance in certain clinical correlations, such as the direct link between TMB and OS, may be attributed to limited sample size or the

inherent molecular heterogeneity of CESC, necessitating further validation in larger, multicenter, prospective cohorts.

5. Conclusion

While a higher TMB showed a non-significant trend toward improved survival outcomes in the early years of follow-up, its primary impact appears to be the induction of local immune recognition in CESC. Activated $CD4^+$ memory and $CD8^+$ T cells serve as prognostic indicators for CESC. The *PTGS2* gene emerges as a noteworthy immune-related candidate in CESC, representing a potential, albeit preliminary, biomarker. Given the moderate predictive performance of our current model, further integration of multi-omics data and large-scale prospective clinical trials are necessary to refine its utility and ascertain its definitive therapeutic potential. Our study utilized the CIBERSORT method to estimate the proportion of immune cells in each CESC patient, necessitating foundational experiments to verify the association between the *PTGS2* gene and immune cell infiltration. Additionally, large-scale clinical studies are needed to validate the prognostic effect of TMB and its potential relationship with immune cell infiltration in the future.

Acknowledgments

The authors would like to express their sincere gratitude to Mr. Yufeng Tian from the School of Mathematics and Physics, University of Science and Technology Beijing, for his valuable statistical consultation and expert assistance in the processing and analysis of the CGCI–HTMCP–CC from the Genomic Data Commons Data Portal (GDC) database (https://portal.gdc.cancer.gov/) and transcriptomic data of cervical patients from local cohorts.

Funding

This research was funded by the Fundamental Research Funds for the Central Universities (grant number: DUT22YG107), the National Natural Science Foundation of China (grant number: 81600370), and the China Postdoctoral Science Foundation (grant number: 2018M640270) for Yanshuo Han. It is also funded by the CMU High-Quality Development Foundation of the Liaoning Provincial Science and Technology Department (No. 2023JH2/20200164) for Shutao Tan.

Conflict of interest

The authors declare no conflicts of interest.

Author contributions

Conceptualization: Batchimeg Tsedenbal, Bayarmaa Enkhbat, Yanshuo Han

Data curation: Batchimeg Tsedenbal, Haiqing Jia, Zhenyong Yang, Yanshuo Han

Formal analysis: Yunfeng Dai, Battogtokh Chimeddorj, Haiqing Jia

Investigation: Batchimeg Tsedenbal, Zhenyong Yang, Yun Li, Yanshuo Han

Methodology: Battogtokh Chimeddorj, Shutao Tan, Yun Li

Project administration: Batchimeg Tsedenbal, Shutao Tan, Yanshuo Han

Supervision: Batchimeg Tsedenbal, Shutao Tan, Yanshuo Han

Writing–original draft: Battogtokh Chimeddorj, Haiqing Jia

Writing–review & editing: Batchimeg Tsedenbal, Yanshuo Han

Ethics approval and consent to participate

Not applicable.

Consent for publication

Not applicable.

Availability of data

The raw data supporting the findings of this study are available in the TCGA (https://portal.gdc.cancer.gov/) and CGCI (https://ocg.cancer.gov/programs/cgci) databases. The custom R scripts used for TMB calculation, maxstat thresholding, and risk-score modeling have been archived and are available from the corresponding author upon reasonable request to ensure the reproducibility of our findings.

References

1. Goodman A. HPV testing as a screen for cervical cancer. *BMJ.* 2015;350:june30 1:h2372.

   doi: 10.1136/bmj.h2372

2. Sung H, Ferlay J, Siegel RL, *et al.* Global Cancer Statistics 2020: GLOBOCAN Estimates of Incidence and Mortality Worldwide for 36 Cancers in 185 Countries. *CA Cancer J Clin.* 2021;71(3):209-249.

   doi: 10.3322/caac.21660

3. Mezache L, Paniccia B, Nyinawabera A, Nuovo GJ. Enhanced expression of PD L1 in cervical intraepithelial neoplasia and cervical cancers. *Mod Pathol.* 2015;28(12):1594-1602.

   doi: 10.1038/modpathol.2015.108

4. Chan TA, Yarchoan M, Jaffee E, *et al.* Development of tumor mutation burden as an immunotherapy biomarker: utility for the oncology clinic. *Ann Oncol.* 2019;30(1):44-56.

   doi: 10.1093/annonc/mdy495

5. Lheureux S, Butler MO, Clarke B, *et al.* Association of Ipilimumab With Safety and Antitumor Activity in Women With Metastatic or Recurrent Human Papillomavirus-Related Cervical Carcinoma. *JAMA Oncol.* 2018;4(7):e173776.

doi: 10.1001/jamaoncol.2017.3776

6. Rajpoot A, Sharma V. Bridging Cancer and Cardiovascular Health: A Comprehensive Review of Cardiotoxicity in Modern Oncology. *Heart Mind.* 2025;9(2):115-135.

doi: 10.4103/hm.HM-D-24-00148

7. Tam CWL, Yam JWP. Harnessing the potential of small extracellular vesicle biomarkers for cancer diagnosis and prognosis with advanced analytical technologies. *J Transl Int Med.* 2025;13(3):187-200.

doi: 10.1515/jtim-2025-0019

8. Buttner R, Longshore JW, Lopez-Rios F, *et al.* Implementing TMB measurement in clinical practice: considerations on assay requirements. *ESMO Open.* 2019;4(1):e000442.

doi: 10.1136/esmoopen-2018-000442

9. An H, Cheng X, Xue L, *et al.* Genomic Instability is Widespread in Esophageal Squamous Dysplasia and Increases During the Progression to Cancer. *Front Biosci (Landmark Ed).* 2025;30(10):41107.

doi: 10.31083/FBL41107

10. Jardim DL, Goodman A, de Melo Gagliato D, Kurzrock R. The Challenges of Tumor Mutational Burden as an Immunotherapy Biomarker. *Cancer Cell.* 2021;39(2):154-173.

doi: 10.1016/j.ccell.2020.10.001

11. Gandara DR, Paul SM, Kowanetz M, *et al.* Blood-based tumor mutational burden as a predictor of clinical benefit in non-small-cell lung cancer patients treated with atezolizumab. *Nat Med.* 2018;24(9):1441-1448.

doi: 10.1038/s41591-018-0134-3

12. Lumish MA, Cercek A. Immunotherapy for the treatment of colorectal cancer. *J Surg Oncol.* 2021;123(3):760-774.

doi: 10.1002/jso.26357

13. Kim B, Kang SY, Kim KM. DNA-protein biomarkers for immunotherapy in the era of precision oncology. *J Pathol Transl Med.* 2021;55(1):26-32.

doi: 10.4132/jptm.2020.09.23

14. Griewing LM, Schweizer C, Schubert P, *et al.* Questionnaire-based detection of immune-related adverse events in cancer patients treated with PD-1/PD-L1 immune checkpoint inhibitors. *BMC Cancer.* 2021;21(1):314.

doi: 10.1186/s12885-021-08006-0

15. Galvano A, Gristina V, Malapelle U, *et al.* The prognostic impact of tumor mutational burden (TMB) in the first-line management of advanced non-oncogene addicted non-small-cell lung cancer (NSCLC): a systematic review and meta-analysis of randomized controlled trials. *ESMO Open.* 2021;6(3):100124.

doi: 10.1016/j.esmoop.2021.100124

16. Hofman P. Next-Generation Sequencing with Liquid Biopsies from Treatment-Naive Non-Small Cell Lung Carcinoma Patients. *Cancers.* 2021;13(9):2049.

doi: 10.3390/cancers13092049

17. Budczies J, Seidel A, Christopoulos P, *et al.* Integrated analysis of the immunological and genetic status in and across cancer types: impact of mutational signatures beyond tumor mutational burden. *Oncoimmunology.* 2018;7(12):e1526613.

doi: 10.1080/2162402X.2018.1526613

18. Mohammed RK, Alrawi ATH, Dawood AJ. A dual-approach to genomic predictions: leveraging convolutional networks and voting classifiers. *Biomed Eng Commun.* 2025;4(1):02.

doi: 10.53388/BMEC2025002

19. Singh RR, Patel KP, Routbort MJ, *et al.* Clinical validation of a next-generation sequencing screen for mutational hotspots in 46 cancer-related genes. *J Mol Diagn.* 2013;15(5):607-622.

doi: 10.1016/j.jmoldx.2013.05.003

20. Zhou M, Zhou M, Jin Y. Tumour Cell Size Control and Its Impact on Tumour Cell Function. *Cell Prolif.* 2025;58(12):e70080.

doi: 10.1111/cpr.70080

21. Balar AV, Galsky MD, Rosenberg JE, *et al.* Atezolizumab as first-line treatment in cisplatin-ineligible patients with locally advanced and metastatic urothelial carcinoma: a single-arm, multicentre, phase 2 trial. *Lancet.* 2017;389(10064):67-76.

doi: 10.1016/S0140-6736(16)32455-2

22. Buchhalter I, Rempel E, Endris V, *et al.* Size matters: Dissecting key parameters for panel-based tumor mutational burden analysis. *Int J Cancer.* 2019;144(4):848-858.

doi: 10.1002/ijc.31878

23. Zehir A, Benayed R, Shah RH, *et al.* Mutational landscape of metastatic cancer revealed from prospective clinical sequencing of 10,000 patients. *Nat Med.* 2017;23(6):703-713.

doi: 10.1038/nm.4333

24. Li X, Liu A, Mu X, *et al.* Computational analyses to reveal the key determinants of the high malignancy level of cholangiocarcinoma. *J Transl Int Med.* 2024;12(6):602-617.

doi: 10.1515/jtim-2024-0033

25. Ritchie ME, Phipson B, Wu D, *et al.* limma powers differential expression analyses for RNA-sequencing and microarray studies. *Nucleic Acids Res.* 2015;43(7):e47.

doi: 10.1093/nar/gkv007

26. Wang R, Pan W, Jin L, *et al*. Human papillomavirus vaccine against cervical cancer: Opportunity and challenge. *Cancer Lett*. 2020;471:88-102.

doi: 10.1016/j.canlet.2019.11.039

27. Ferrall L, Lin KY, Roden RBS, Hung CF, Wu TC. Cervical Cancer Immunotherapy: Facts and Hopes. *Clin Cancer Res*. 2021;27(18):4953-4973.

doi: 10.1158/1078-0432.CCR-20-2833

28. Ma YY, Wei SJ, Lin YC, *et al*. PIK3CA as an oncogene in cervical cancer. *Oncogene*. 2000;19(23):2739-2744.

doi: 10.1038/sj.onc.1203597

29. Wright AA, Howitt BE, Myers AP, *et al*. Oncogenic mutations in cervical cancer: genomic differences between adenocarcinomas and squamous cell carcinomas of the cervix. *Cancer*. 2013;119(21):3776-3783.

doi: 10.1002/cncr.28288

30. Kamal M, Lameiras S, Deloger M, *et al*. Human papilloma virus (HPV) integration signature in Cervical Cancer: identification of MACROD2 gene as HPV hot spot integration site. *Br J Cancer*. 2021;124(4):777-785.

doi: 10.1038/s41416-020-01153-4

31. Husseinzadeh N, Husseinzadeh HD. mTOR inhibitors and their clinical application in cervical, endometrial and ovarian cancers: a critical review. *Gynecol Oncol*. 2014;133(2):375-381.

doi: 10.1016/j.ygyno.2014.02.017

32. Savarese M, Maggi L, Vihola A, *et al*. Interpreting Genetic Variants in Titin in Patients With Muscle Disorders. *JAMA Neurol*. 2018;75(5):557-565.

doi: 10.1001/jamaneurol.2017.4899

33. Chen P, Wang R, Yue Q, Hao M. Long non-coding RNA TTN-AS1 promotes cell growth and metastasis in cervical cancer via miR-573/E2F3. *Biochem Biophys Res Commun*. 2018;503(4):2956-2962.

doi: 10.1016/j.bbrc.2018.08.077

34. Park SE, Park K, Lee E, *et al*. Clinical implication of tumor mutational burden in patients with HER2-positive refractory metastatic breast cancer. *Oncoimmunology*. 2018;7(8):e1466768.

doi: 10.1080/2162402X.2018.1466768

35. Samstein RM, Lee CH, Shoushtari AN, *et al*. Tumor mutational load predicts survival after immunotherapy across multiple cancer types. *Nat Genet*. 2019;51(2):202-206.

doi: 10.1038/s41588-018-0312-8

36. Liu S, Kang M, Ren Y, *et al*. The Interaction Between Vasculogenic Mimicry and the Immune System: Mechanistic Insights and Dual Exploration in Cancer Therapy. *Cell Prolif*. 2025;58(6):e13814.

doi: 10.1111/cpr.13814

37. Zheng X, Ke F, Yao M, *et al*. Biophysical Properties of the Extracellular Matrix in Cancer: Insights Into Immunotherapy. *Front Biosci (Landmark Ed)*. 2025;30(10):44127.

doi: 10.31083/FBL44127

38. Pages F, Kirilovsky A, Mlecnik B, *et al*. In situ cytotoxic and memory T cells predict outcome in patients with early-stage colorectal cancer. *J Clin Oncol*. 2009;27(35):5944-5951.

doi: 10.1200/JCO.2008.19.6147

39. Garcia-Martinez E, Gil GL, Benito AC, *et al*. Tumor-infiltrating immune cell profiles and their change after neoadjuvant chemotherapy predict response and prognosis of breast cancer. *Breast Cancer Res*. 2014;16(6):488.

doi: 10.1186/s13058-014-0488-5

40. Matsumoto H, Thike AA, Li H, *et al*. Increased CD4 and CD8-positive T cell infiltrate signifies good prognosis in a subset of triple-negative breast cancer. *Breast Cancer Res Treat*. 2016;156(2):237-247.

doi: 10.1007/s10549-016-3743-x

41. Masson-Lecomte A, Rava M, Real FX, Hartmann A, Allory Y, Malats N. Inflammatory biomarkers and bladder cancer prognosis: a systematic review. *Eur Urol*. 2014;66(6):1078-1091.

doi: 10.1016/j.eururo.2014.07.033

42. Sato E, Olson SH, Ahn J, *et al*. Intraepithelial CD8+ tumor-infiltrating lymphocytes and a high CD8+/regulatory T cell ratio are associated with favorable prognosis in ovarian cancer. *Proc Natl Acad Sci USA*. 2005;102(51):18538-18543.

doi: 10.1073/pnas.0509182102

43. Li MY, Zhang H, Li J, *et al*. Reshaping the future of cancer therapy: taming toxicity and side effects. *Biomed Eng Commun*. 2026;5(2):11.

doi: 10.53388/BMEC2026011